
UNCONDITIONAL LATENT DIFFUSION MODELS MEMORIZE PATIENT IMAGING DATA: IMPLICATIONS FOR OPENLY SHARING SYNTHETIC DATA

Salman Ul Hassan Dar^{1,2,3} **Marvin Seyfarth**¹ **Jannik Kahmann**⁴ **Isabelle Ayx**⁴
Theano Papavassiliu^{2,3,5} **Stefan O. Schoenberg**^{2,4} **Norbert Frey**^{1,3} **Bettina Baeßler**⁶
Sebastian Foersch⁷ **Daniel Truhn**⁸ **Jakob Nikolas Kather**^{9,10,11} **Sandy Engelhardt**^{1,2,3}

¹Department of Internal Medicine III, Heidelberg University Hospital, Germany

²AI Health Innovation Cluster (AIH), Germany

³German Centre for Cardiovascular Research (DZHK), Partner site Heidelberg/Mannheim, Germany

⁴Department of Radiology and Nuclear Medicine, University Medical Center Mannheim, Germany

⁵Department of Cardiology, Angiology, Hemostasis, and Medical Intensive Care,
University Medical Centre Mannheim, Medical Faculty Mannheim, University of Heidelberg, Germany.

⁶Department of Diagnostic and Interventional Radiology,
University Hospital Würzburg, Oberdürrbacher Str. 6, 97080 Würzburg, Germany.

⁷Institute of Pathology, University Medical Center Mainz, Mainz, Germany

⁸Diagnostic and Interventional Radiology, University Hospital Aachen, Aachen, Germany

⁹Else Kroener Fresenius Center for Digital Health, Medical Faculty Carl Gustav Carus,
TUD Dresden University of Technology, Dresden, Germany

¹⁰Department of Medicine I, University Hospital Dresden, Dresden, Germany

¹¹Medical Oncology, National Center for Tumor Diseases (NCT), University Hospital Heidelberg,
Heidelberg, Germany

July 16, 2024

ABSTRACT

AI models present a wide range of applications in the field of medicine. However, achieving optimal performance requires access to extensive healthcare data, which is often not readily available. Furthermore, the imperative to preserve patient privacy restricts patient data sharing with third parties and even within institutes. Recently, generative AI models have been gaining traction for facilitating open-data sharing by proposing synthetic data as surrogates of real patient data. Despite the promise, these models are susceptible to patient data memorization, where models generate patient data copies instead of novel synthetic samples. This undermines the whole purpose of preserving patient data privacy and may even result in patient re-identification. Considering the importance of the problem, surprisingly it has received relatively little attention in the medical imaging community. To this end, we assess memorization in unconditional latent diffusion models, which are the building blocks of some of the most advanced generative AI models. We train 2D and 3D latent diffusion models on CT, MR, and X-ray datasets for synthetic data generation. Afterwards, we detect the amount of training data memorized utilizing our self-supervised approach and further investigate various factors that can influence memorization by training models in different settings. Our findings show a surprisingly high degree of patient data memorization across all datasets, with approximately 40.9% of patient data being memorized and 78.5% of synthetic samples identified as patient data copies on average

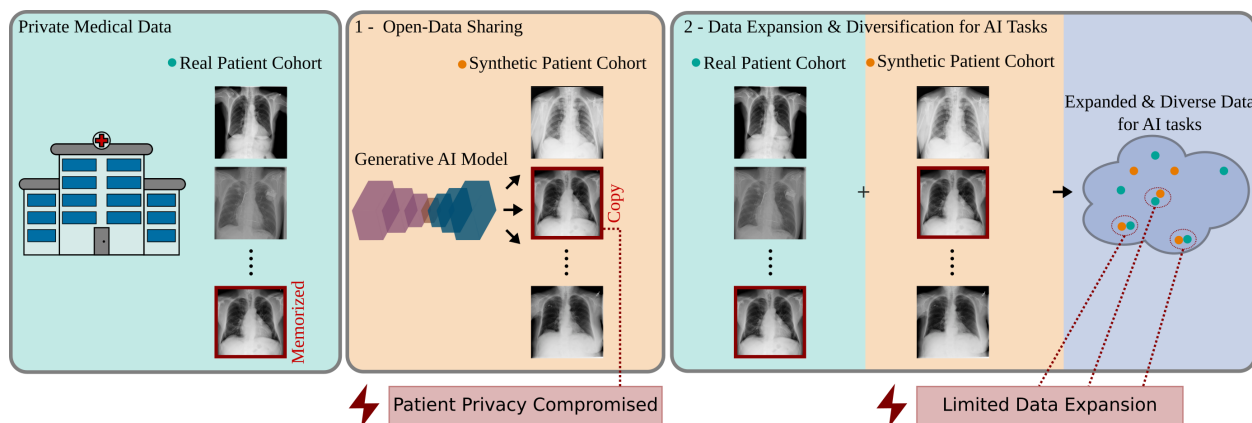


Figure 1: Generative models are first trained on private medical data. These models can be used to synthesize novel samples, which can have multiple applications. 1) Open-data sharing: Synthesized samples can be shared publicly for advancing medical imaging research while preserving patient privacy. However, synthesized samples can be patient data replicas, thereby compromising patient privacy. 2) Data Expansion and Diversification - Synthetic samples can be utilized to expand and diversify the training data. Nevertheless, if most of the synthetic samples are patient data replicas, the expansion and diversification is likely to be limited.

in our experiments. Further analyses reveal that using augmentation strategies during training can reduce memorization while over-training the models can enhance it. Although increasing the dataset size does not reduce memorization and might even enhance it, it does lower the probability of a synthetic sample being a patient data copy. Collectively, our results emphasize the importance of carefully training generative models on private medical imaging datasets, and examining the synthetic data to ensure patient privacy before sharing it for medical research and applications.

Keywords Memorization · Contrastive Learning · Latent Diffusion · Patient Privacy

1 Introduction

Recent developments in artificial intelligence (AI) hold the potential to transform the current healthcare system. AI models are generally data-hungry, necessitating the healthcare data to scale with the contemporary AI models. While this could be alleviated via patient data sharing among multiple imaging sites and research centers, concerns regarding patient privacy render it infeasible. Modern developments in generative deep diffusion probabilistic models have led to a significant leap in performance level in various medical imaging applications [1, 2, 3, 4], a notable application being open data sharing [5, 6, 7, 8, 9]. In open-data sharing, generative models are first trained to learn data distribution from private medical imaging datasets. Afterwards, these generative models are used to generate synthetic samples, and since these synthesized samples do not belong to any specific patient, they can be shared publicly without compromising patient privacy (Fig. 1). As a matter of fact, very recently, several studies have trained generative models on private/limited-access/restricted datasets and made synthetic data [5] or trained generative models [10, 11] publicly available.

Despite the potential of generative models for open data sharing, an underlying assumption is that the generated samples are novel and not mere patient data replicas. This is crucial, as the primary motivation for using synthetic data as surrogates of real patient data is to preserve patient privacy and synthesizing patient data copies circumvents the goal. A synthesized copy can even be traced back to the original patient, leading to patient re-identification [12]. Given the sensitive nature of patient medical data, surprisingly there has been little focus on the threat of such models to memorize training data and detect those memorized training samples efficiently.

Detecting memorized samples in the training data can be challenging. Identifying whether a sample is memorized requires comparing it with all synthesized samples, which is sub-optimal both in terms of computational complexity and detection performance. For instance, if a synthesized sample is a slightly rotated copy of a training sample, their pixel-wise differences could still be significant and the patient data copy might go undetected. For this purpose, copy detection can be performed via self-supervised models trained based on contrastive learning. In such models, copy detection is performed in a low dimensional embedding space, which makes the whole process computationally efficient and further enables the detection of copies among the synthesized samples that are variants such as rotated versions of the training samples. Such models have been demonstrated for patient re-identification and copy detection in 2D X-ray

images [12, 13]. However, such applications in 3D medical images have yet to be demonstrated.

While training generative models, the emphasis is typically on improving validation errors or metrics that quantify image quality [14] or diversity [15], without taking into consideration the memorization capacities of such models. Despite their widespread usage, the commonly used metrics have inherent limitations [16], and give no direct information regarding patient data memorization. Likewise, the validation loss itself only provides auxiliary information regarding model training and can even show a negative correlation with data memorization [17]. This also makes it challenging to determine an appropriate number of training steps. In fact, over-training is one of the several factors that could influence memorization, and other factors like training data size and data augmentation can also have an impact on memorization [18, 19]. Therefore, exploring memorization-informed model training and metrics is crucial [16].

Here, we thoroughly investigate memorization in unconditional latent diffusion models (LDMs) for medical imaging. LDMs learn data generation in the low-dimensional latent space of an autoencoder, which makes them computationally efficient while preserving high image quality.[20]. Understanding memorization in unconditional LDMs is important since they form the foundation of advanced multi-modal and conditional generative AI tools such as stable diffusion, which typically adapt pre-trained unconditional LDMs or perform hybrid training with unconditional LDMs [20, 21]. We train unconditional LDMs on medical images to learn data distributions and perform patient data copy detection among the synthesized samples using self-supervised models.

As a means to understand memorization in unconditional diffusion models, we pose the following questions regarding memorization in LDMs for medical image synthesis:

Prevalence: Is memorization equally prevalent in 2D and 3D LDMs, as well as in medical images with varying properties such as organs, dimension, resolution, field-of-view, contrast, and modality? (section 2.2)

Efficient Detection: How can patient data memorization be efficiently detected? (section 2.3)

Impact of Training Data Size: How is memorization affected by the training data size? (section 2.4.1)

Memorization as a Metric: Can memorization be used as a metric to assess generative models during training? (section 2.4.2)

Comparison with Traditional Metrics: Can a link between memorization and traditional metrics for assessing generative models be established? (section 2.4.2)

Mitigation via Data Augmentation: Can data memorization be alleviated by data augmentation during model training? (section 2.4.3)

2 Results

2.1 Experimental Settings

Datasets We performed a thorough assessment of memorization in unconditional latent diffusion models (LDMs) by conducting analyses on three medical imaging datasets covering a range of modalities, organs, image resolution, fields of view, and spatial dimensions. We conducted experiments on 3D volumes from a publicly available knee MRI dataset (MRNet) [22], 3D sub-volumes surrounding plaques from an in-house photon counting coronary computed tomography angiography dataset (PCCTA), and 2D images from a publicly available X-ray dataset [23]. In the MRNet dataset, 904 volumes were used for training and 226 for validation. In the PCCTA dataset, 242 volumes were used for training and 58 for validation. In the X-ray dataset, 10k images were reserved for training and 10k for validation.

Generative Models For 3D datasets, Medical Diffusion (MedDiff) [24] and Medical Open Network for Artificial Intelligence (MONAI) [25] based LDMs were adopted. For the X-ray dataset, a Medical Open Network for Artificial Intelligence (MONAI-2D) based LDM was adopted. LDMs were trained on all datasets separately. Afterward, each model was used to synthesize novel samples. These synthesized samples were then categorized as novel or copies using self-supervised models (see section 4.2 for details). We opted for MedDiff and MONAI because they are based on some of the most widely used repositories for LDMs-based medical image synthesis.

Memorization We considered two aspects of memorization. First, we assess the number of training samples memorized. This constitutes the number of training samples that are synthesized as patient data replicas among the synthetic samples (N_{mem}). Second, we look at the number of synthetic samples that are patient data replicas (N_{copies}). N_{copies} is always greater than or equal to N_{mem} because a patient data replica can be repeated multiple times in the synthesized data.

2.2 Memorization Prevalence

Theoretically, a model that perfectly learns the data distribution always has a non-zero probability of generating patient data copies. As a result, a synthetic dataset with an infinite number of generated samples would eventually include all

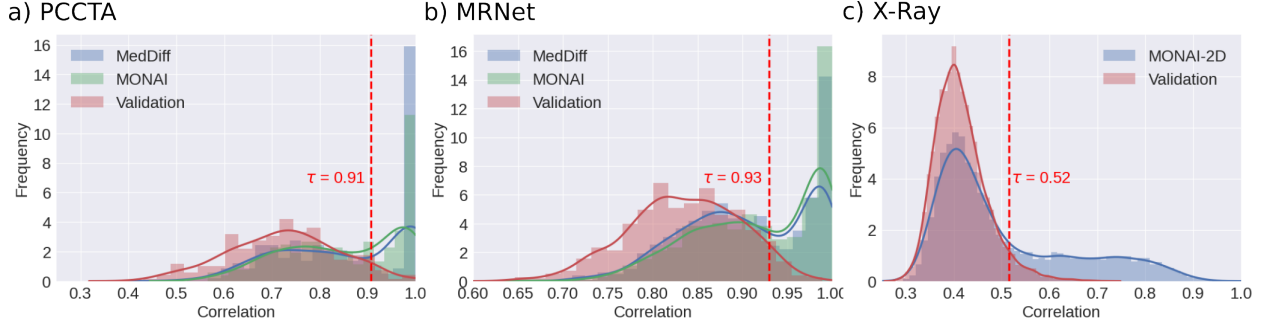


Figure 2: Histograms showing distributions of Pearson’s correlation values among closest training-validation pairs and training-synthetic pairs in a) PCCTA, b) MRNet, and c) X-ray datasets. All training, validation, and synthetic samples were projected onto embedding space using self-supervised models. For each training embedding, closest embedding was selected from the validation data denoted as ‘Validation’, MONAI-synthesized data denoted as ‘MONAI’, MedDiff-synthesized data denoted as ‘MedDiff’, and 2D MONAI-synthesized data denoted as ‘MONAI-2D’. Afterwards, τ was selected based on the 95th percentile of the correlation values in ‘Validation’ in each dataset, and synthetic samples with correlation values greater than τ were classified as copies.

training samples. Therefore, the critical question is determining how frequently the model generates patient data copies. To answer this question, we synthesized a finite number of samples (N_{syn}) by setting it equal to the training data size (N_{train}). LDMs trained on each dataset were used to synthesize novel images. Afterwards, self-supervised models were used to detect potential replicas of training samples among the synthesized samples. These self-supervised models first project the training, validation, and synthetic data onto a lower dimensional embedding space. This projection makes the copy detection process computationally efficient and further enables us to detect copies that are not just identical to the training samples but are also variations of the real samples such as flipping, rotation, and slight changes in contrast. Next, Pearson’s correlation coefficient reflecting similarity was computed between all pairs of training-validation and training-synthetic embeddings. Afterward, for each training embedding the closest validation and nearest synthetic embeddings (ρ_{NN-val}), and between training and nearest synthetic embeddings (ρ_{NN-syn}) in both MedDiff and MONAI. In all datasets and models, ρ_{NN-syn} values were shifted more towards the right compared to ρ_{NN-val} values, implying that synthetic samples bear a higher resemblance to the training data.

Next, we quantified the number of training samples memorized (N_{mem}) by the model and the number of synthesized samples that were copies (N_{copies}) based on a correlation threshold value τ (for details please refer to Section. 4.2.2). The numbers are reported in Fig. 3. In PCCTA dataset, (43.8, 40.5) % of the training data were memorized in (MedDiff, MONAI), and (91.7, 83.1) % of the synthetically generated samples were identified as patient data copies in (MedDiff, MONAI). Fig. 4 shows copies that were detected in both MedDiff and MONAI along with the closest training samples. In the PCCTA dataset, which contains low-dimensional 3D patches, most of the details were preserved in the memorized samples, and in terms of quality, both MedDiff and MONAI generated images of similar quality.

In MRNet dataset, (40.2, 47.6) % of the training data were memorized in (MedDiff, MONAI), and (76.1, 87.2) % of the synthetically generated samples were identified as patient data copies in (MedDiff, MONAI). Fig. 5 shows copies that were detected in both MedDiff and MONAI along with the closest training samples. In the MRNet dataset, which contained full 3D volumes, most of the global structure was preserved, albeit with notable differences in fine structural details between MedDiff and MONAI. MedDiff-synthesized images were noisy and unable to capture low-level structural details (Supp. Fig. S1). MONAI-synthesized images, on the other hand, had a lower noise level but were slightly blurry (Supp. Fig. S1). In MRNet, while both networks produced patient data copies, both models were unable to generate small structural details.

In the 2D X-ray dataset, 32.6 % of the training data were memorized and 54.5% of the synthetic samples were patient data copies in MONAI-2D. Fig. 6 shows copies alongside the closest training samples. Synthetic samples show a very close resemblance to the training samples. Overall, we observed a high level of patient data was memorized in both 2D and 3D models. Moreover, a very large percentage of synthesized samples were patient data copies, especially in 3D models.

2.3 Efficient Copy Detection

Next, we gauged the effectiveness of the self-supervised models in detecting copies. The correlation threshold τ used to categorize samples as copy or novel was based on the 95th percentile of the correlation values between training and

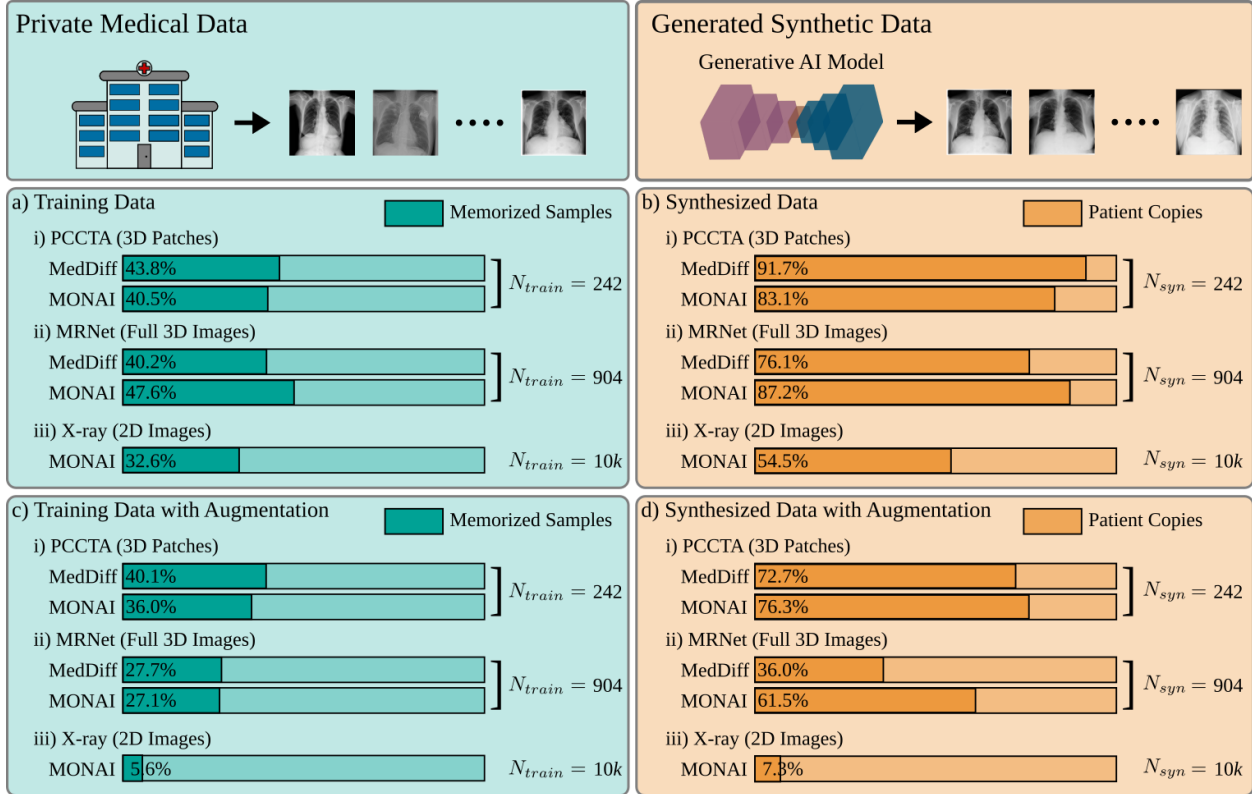


Figure 3: The left column represents private training data, and the right column represents synthesized data. a) Number of memorized training samples (N_{mem}) and b) synthesized samples that are patient data copies (N_{copies}) in PCCTA, MRNet, and X-ray datasets. All datasets show a high percentage of N_{mem} and N_{copies} , notably in 3D datasets. Percentage c) N_{mem} and d) N_{copies} are shown in the models trained with data augmentation. Augmentation during training reduces patient data memorization. However, it can come at the expense of compromise in image quality. For instance, there is a drastic reduction in the percentage of N_{copies} in the MedDiff-synthesized sample in the MRNet dataset. However, visual inspection (Supp. Fig. S1) shows that the model is unable to synthesize realistic high-quality images.

nearest validation sample embeddings (Fig. 2). To evaluate if the selected threshold value τ was meaningful, we also randomly selected 100 training and nearest synthetic sample pairs, and manually labeled the corresponding synthesized samples as novel or copies. These labels were then compared with the ones obtained based on τ . In the PCCTA dataset, copies were detected with sensitivity of 89% and specificity of 81% among the MedDiff-synthesized samples and with sensitivity of 98% and specificity of 84% among MONAI-synthesized samples. In the MRNet dataset, copies were detected with sensitivity of 85% and specificity of 97% in the MedDiff-synthesized samples and with sensitivity of 84% and specificity of 100% in the MONAI-synthesized samples. In the X-ray dataset, copies were detected with sensitivity of 85% and specificity of 94% in the MONAI-2D synthesized samples. These values reflect the effectiveness of the copy detection pipeline.

2.4 Factors Affecting Memorization

Next, we investigated the factors that could potentially influence memorization. For this purpose, we considered three different aspects including training data size, training iterations and data augmentation.

2.4.1 Impact of Training Data Size

Deep neural networks are prone to overfitting upon training on small datasets. Although overfitting and memorization are distinct concepts, overfitting can lead to memorization. LDMs learn data generation through gradual denoising, an inherently ill-posed problem with infinitely many solutions. Training LDMs on small datasets makes the models overfit to solutions, leading to denoised training images. This can in turn increase the likelihood of generating more

training samples at random. To explore this phenomenon, we investigated the effect of training data size (N_{train}) on memorization in the X-ray dataset, the main reason being that it is a large dataset and provides us with the freedom to select different numbers of training samples. We compared the LDMs trained for $N_{train} = (5k, 10k, 20k)$ images denoted as ($G_{\theta,5k}, G_{\theta,10k}, G_{\theta,20k}$) respectively. We maintained the number of epochs at 3k for all three models to ensure that each model encountered each training sample the same number of times. The self-supervised model was trained on 20k training images. Fig. 7 shows the percentage of training samples that were memorized and the percentage of synthesized samples that were patient data copies. (54.7, 33.2, 17.7)% of the training samples were memorized in ($G_{\theta,5k}, G_{\theta,10k}, G_{\theta,20k}$) and (68.6, 51.4, 39.9)% of the synthesized samples were copies in ($G_{\theta,5k}, G_{\theta,10k}, G_{\theta,20k}$). Supp. Fig. S2 also shows distributions among correlation values of training samples and nearest synthetic samples along with the corresponding mean values. Increasing the training set size reduced the percentage of memorized training data samples. However, surprisingly, there was a slight increase in number of memorized training samples (N_{mem}) with the increase in the number of training samples (N_{train}), with N_{mem} equal to (2.7k, 3.3k, 3.5k) in ($G_{\theta,5k}, G_{\theta,10k}, G_{\theta,20k}$). More interestingly, the number of synthesized samples that were patient data copies (N_{copies}) correlated negatively with N_{train} . This suggests that although the number of memorized samples does not decrease for the models trained on larger data sizes and might even increase, the probability of observing a patient data copy among the synthesized samples decreases with increasing training data size.

2.4.2 Memorization as a Metric

One aspect of LDMs that receives little attention is the number of iterations or epochs used for training, and most of the studies just report a number without performing a thorough evaluation. Overtraining the network can make the network overfit to the training data while denoising, and can lead to more frequent generation of training samples during progressive denoising. This can lead to enhanced memorization [13]. To investigate the effect of training epochs/iterations on memorization of LDMs, we calculated the number of memorized training samples (N_{mem}) as a function of training iterations. Fig. 8c shows N_{mem} detected as a function of training iterations ($N_{iterations}$). In all datasets, N_{mem} increased with training iterations, suggesting that over-training the model can lead to enhanced memorization.

In addition to the relation between N_{mem} and $N_{iterations}$, we were also interested in evaluating their relation with metrics conventionally used for assessment or training of generative models. For this purpose, we also calculated Fréchet inception distance (FID) [14] which measures the quality of the synthesized samples, and multi-scale structural similarity index measure (MS-SSIM) [15] which quantifies diversity among the synthesized samples as a function of

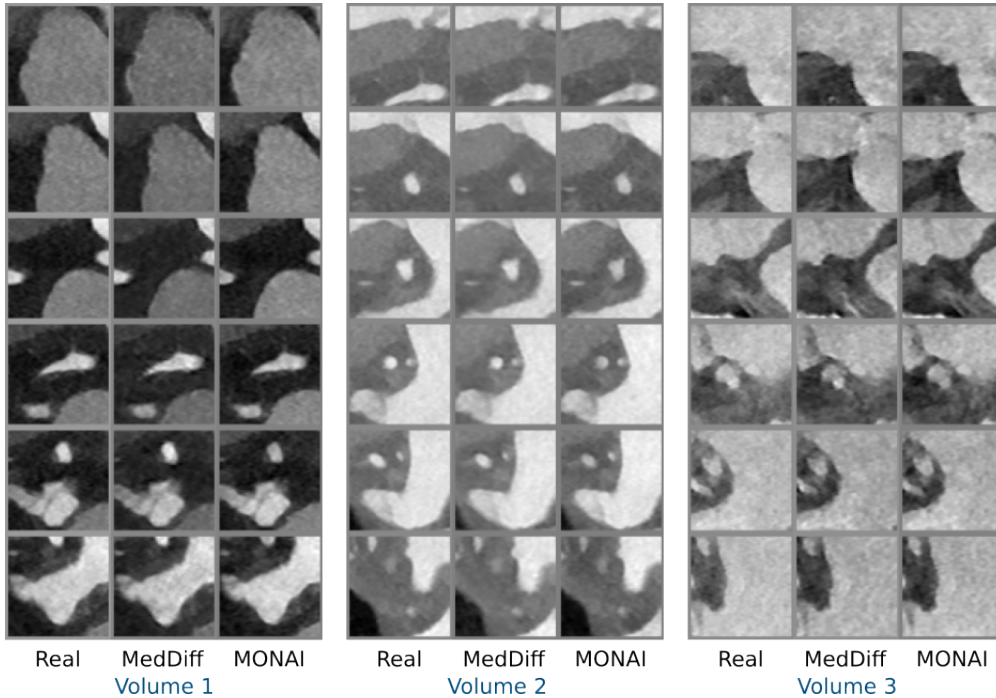


Figure 4: Representative cross sections of real (Real) and copies (MedDiff, MONAI) detected in the PCCTA dataset. Copies show a high resemblance to the corresponding real samples across all slices.

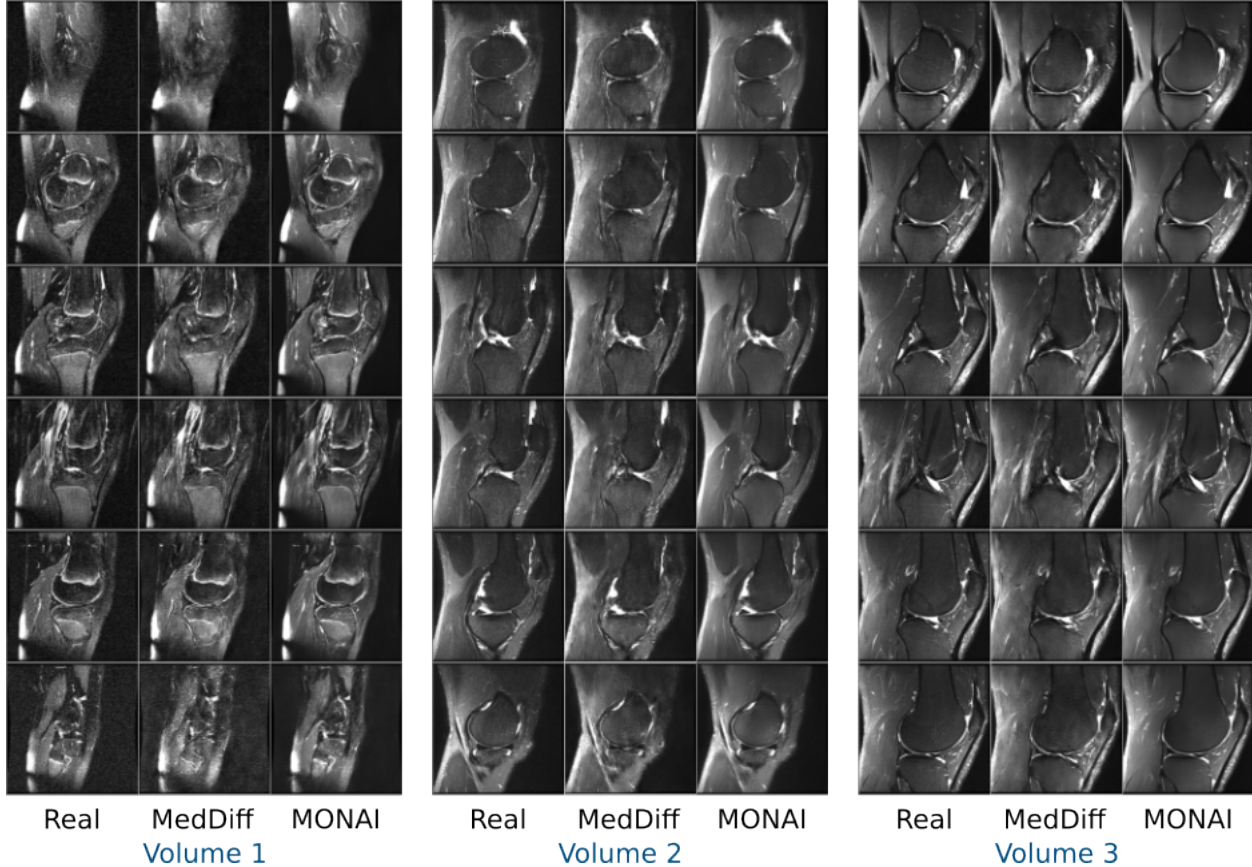


Figure 5: Representative cross sections of real (Real) and copies (MedDiff, MONAI) detected in the MRNet datasets. Copies show a high resemblance to the corresponding real samples.

$N_{iterations}$. Lower FID suggests high quality and low MS-SSIM indicates high diversity. Ideally, we expect FID to decrease and then converge at a point. However, in 3D datasets, FID did not follow a fixed pattern for both models (Fig. 8a) and showed large variations across $N_{iterations}$. This is alarming since FID is perhaps one of the most widely used metrics to assess image quality and compare data-generating capabilities with other models. In the 2D X-ray dataset, FID decreased till 33k iterations and then oscillated afterward. This suggests that image quality saturates after a specific number of iterations. Across all datasets, MS-SSIM did not display a consistent trend (Fig. 8b). Ideally, MS-SSIM should be low, indicating high diversity. However, one thing to consider is that MS-SSIM only quantifies diversity and does not provide any information regarding image quality. In fact, a model generating random noise can have very high diversity. Taken together, our results suggest that traditional measures used to quantify the quality and diversity of the synthesized samples can be misleading and memorization is an aspect that should be taken into account while training generative models, and perhaps a hybrid metric could be used for training models for open-data sharing [16].

2.4.3 Mitigation via Data Augmentation

Data augmentation is a widely used technique that artificially expands the training dataset size by complementing it with variations of training samples. This typically enhances generalizability in deep neural networks, potentially reducing memorization in LDMs [18]. Here, we also assessed memorization in LDMs by training models on expanded datasets obtained via augmentation techniques ($\text{MedDiff}_{\text{Aug}}$, $\text{MONAI}_{\text{Aug}}$). In each epoch, all training samples underwent flipping and rotation (between -5° to 5° along all axes) operations with a probability of 50% each. Fig. 3 compares percentage N_{mem} and N_{copies} in models trained with and without data augmentation.

In the PCCTA dataset, (40.1, 36.0) % of the training data was memorized in ($\text{MedDiff}_{\text{Aug}}$, $\text{MONAI}_{\text{Aug}}$), and (72.7, 76.3) % of the synthetically generated samples were identified as patient data copies in ($\text{MedDiff}_{\text{Aug}}$, $\text{MONAI}_{\text{Aug}}$). This suggests a decrease in memorization in both models. Fig. S3 shows copies that were detected in both $\text{MedDiff}_{\text{Aug}}$ and $\text{MONAI}_{\text{Aug}}$ along with the closest training samples. The copy detection approach is able to capture copies that are also variations of the training samples. In volume 1, the synthesized samples are flipped versions of the training samples,

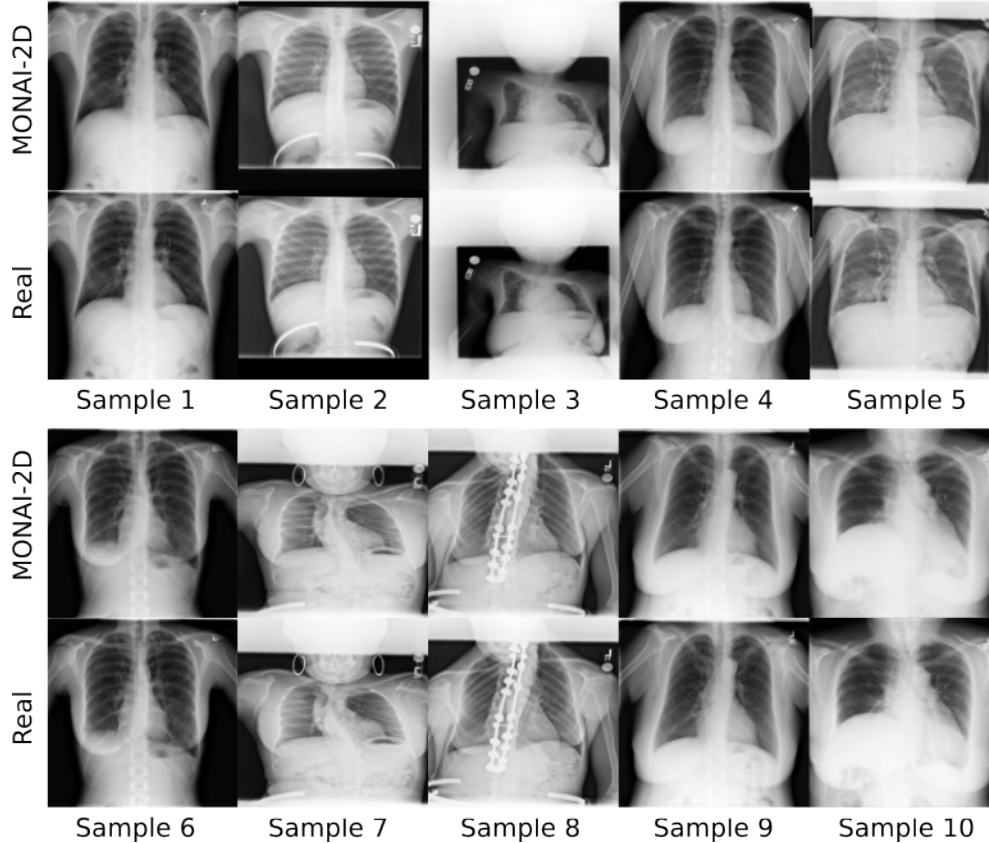


Figure 6: Representative cross sections of real (Real) and copies (MONAI-2D) detected in the X-ray dataset. Copy candidates show a high resemblance to the corresponding real samples. The network tends to copy even the exact position of the image in case of partial field-of-view coverage.

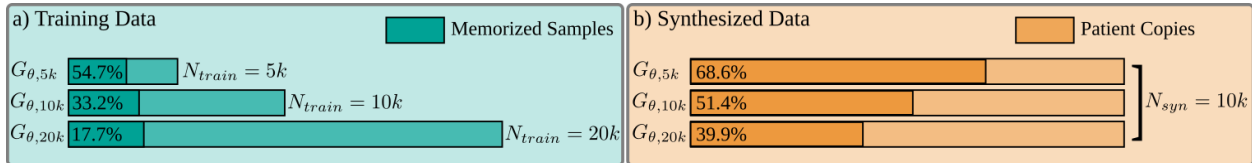


Figure 7: Impact of training data size on the number of a) memorized training samples and b) synthesized samples that are patient data copies.

and in volume 3, MedDiff_{Aug} synthesized sample is flipped and MONAI_{Aug} synthesized sample is a rotated version of the training sample.

In the MRNet dataset, (27.7, 27.1) % of the training data was memorized in (MedDiff_{Aug}, MONAI_{Aug}), and (36.0, 61.5) % of the synthetically generated samples were identified as patient data copies in (MedDiff_{Aug}, MONAI_{Aug}). We also observed a decrease in memorization in the MRNet dataset. Fig. S4 shows copies that were detected in both MedDiff_{Aug} and MONAI_{Aug} along with the closest training samples. The copy detection pipeline was able to detect copies. In MRNet, the samples generated via MedDiff_{Aug} were very poor (Supp. Fig. S1). Although they resemble the corresponding training images globally, they are unable to generate high-quality images. MONAI_{Aug} was able to retain the image quality, however, similar to the models trained without augmentation, we observed slight blurriness induced in the synthesized images.

In the 2D X-ray dataset, 5.6% of the training samples were memorized, and 7.3% of the synthesized samples were copies. This suggests a drastic reduction in memorization compared to the 3D models, which had a significantly smaller training set. Fig. S5 shows some of the selected copies. A careful examination of the copies shows that the patient data copies are not just augmented versions of the original patient image. These copies also contain some notable minor structural variations. One potential explanation is that such models generalize well as they come across different

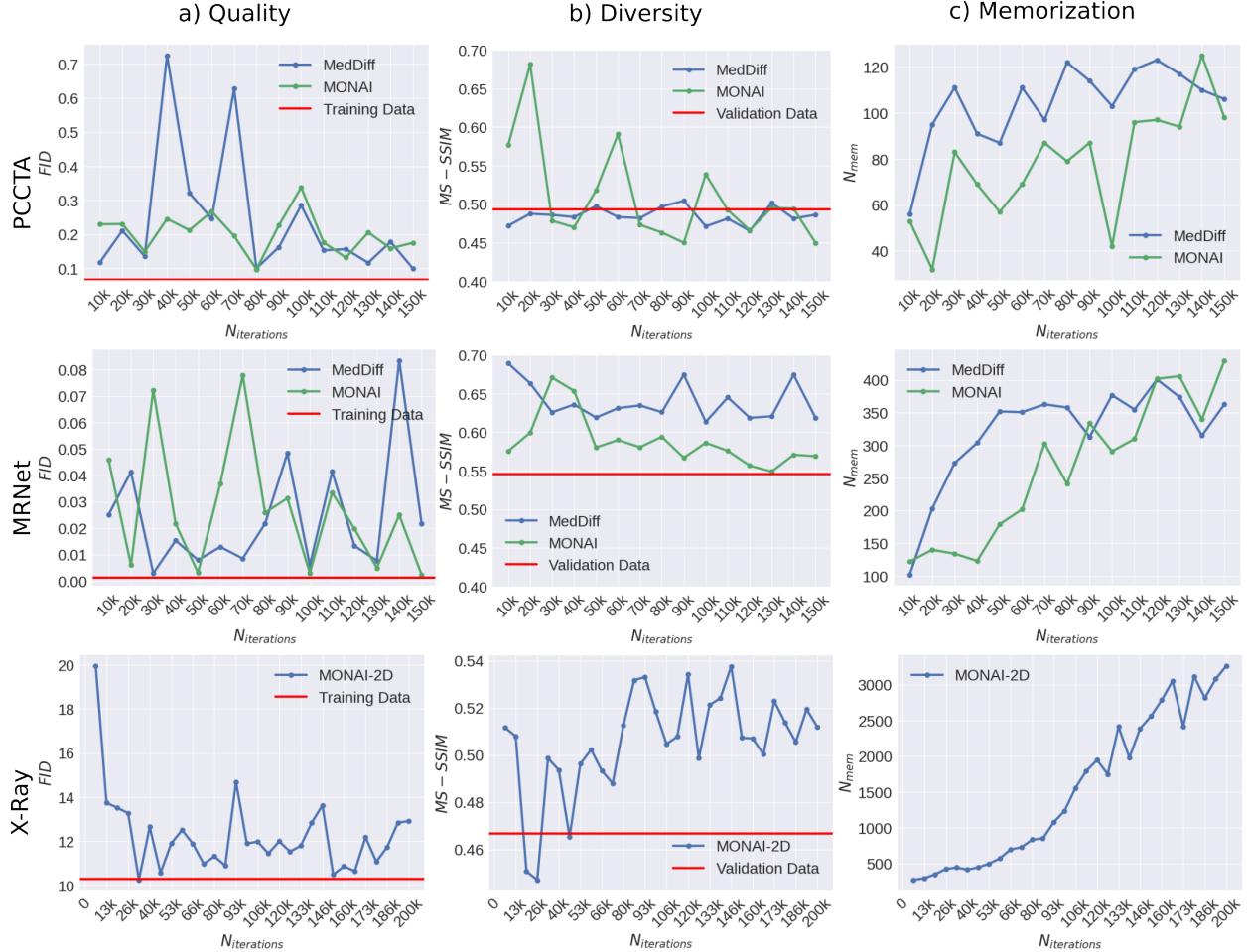


Figure 8: a) Quality assessment metric FID between synthesized (MedDiff, MONAI, MONAI-2D) and real validation images, and between real training (Training Data) and real validation images are shown. b) Diversity assessment metric MS-SSIM within the synthesized data (MedDiff, MONAI, MONAI-2D), and within the validation data (Validation Data) are shown. c) Number of memorized training samples (N_{mem}) among the synthesized samples (MedDiff, MONAI, MONAI-2D) as a function of number of iterations ($N_{iterations}$) used for training are shown.

variations of the training samples and this artificial expansion gives them the ability to generate samples that are not identical to the training samples but interpolations of different variations of the same sample. Another explanation could be related to the way such models are trained. LDMs are trained to perform denoising. In the case of augmentation, the model comes across variations of each training sample multiple times, and instead of finding a solution that produces denoised training images, the model can converge to a solution that is based on minimizing training error across all variations. This in turn can produce images that are not identical to a training sample or its variations, but rather a solution that is an average of all variations. This can potentially lead to the removal or blurriness of small structures. For instance, if we carefully observe samples 2, 3, 8, and 9 (Fig. S5 green markers), we can see that a structure that resembles a wire is present in the training samples but missing from the copies. Furthermore, in samples 1, 2, 4, 5, 6, 8, and 10 (Fig. S5 red markers), the character 'L' at the top right corner is blurred out in the copies.

One intriguing observation is that although we observed a decrease in memorization due to data augmentation during training in both 2D and 3D LDMs, the reduction in memorization was moderate in 3D-LDMs but huge in 2D-LDMs. Furthermore, the synthesized images in 2D-LDMs contained prominent notable variations compared to 3D-LDMs. The underlying reason could be hard to speculate because of differences in model types (2D vs 3D) and dataset features such as training data size, anatomy, and resolution. Overall, we observed that using data augmentation reduced memorization. However, we observed that it could also lead to compromise in image quality.

3 Discussion

In this work, we assessed memorization in unconditional latent diffusion models for medical image synthesis. Trained models were used to synthesize novel medical images, and potential copies were detected using self-supervised models based on the contrastive learning approach. Our results obtained on different datasets covering various organs, resolutions, fields of view, contrasts, and modalities indicate that such models are prone to patient data memorization. Furthermore, our self-supervised models were able to identify copies among synthetic images with reasonable performance levels. Additional complementary analyses point out several factors that can have an impact on memorization. Adding data augmentation operations reduced memorization, whereas over-training enhanced memorization. Increasing the training data size slightly increased the number of memorized samples, however, it decreased the probability of a synthesized sample being a patient data copy. These results suggest that memorization could be mitigated to some extent with careful training.

To date, only a handful of studies have investigated patient data memorization in medical imaging [13, 18, 26]. Akbar et al. [26] assessed memorization in 2D diffusion models, and observed higher pixel-wise correlation among synthetic and real training samples as opposed to real test and training samples. In our previous work [18], we conducted experiments on 3D imaging datasets and utilized contrastive learning for detecting patient data replicas among the synthesized samples in a lower dimensional latent space. In another prior investigation, we showed that overtraining can lead to enhanced memorization [13]. Compared to previous studies, we performed a more thorough assessment of memorization in different datasets, further proposed an approach to detect the memorized training samples, and investigated underlying reasons in different datasets, which could assist in alleviating memorization.

It could be argued that memorization could be mitigated by simply tracking validation error and avoiding over-fitting. However, this assumes equivalency between over-fitting and memorization. While the two terms might sometimes be correlated, this categorization is inaccurate [17]. Over-fitting is a global phenomenon where models attain very high accuracy on the training data typically at the expense of test data accuracy. Memorization, on the other hand, corresponds to the assignment of a very high likelihood to the training data points. As a matter of fact, memorization of a model can be enhanced even when validation loss decreases, especially in the earlier phases of training when memorization might be increasing but the test loss might be decreasing [17].

Our results indicate crucial factors for memorization. Another avenue of research could be devising efficient privacy-preserving generative models. For privacy-preserved open-data sharing, Fernandez et al. [27] proposed a two-step approach. In the first step, a diffusion model was trained on real data and the synthesized samples were refined to contain only novel samples. These refined samples were then utilized to train a new model with the aim to synthesize completely novel data. While this approach reduces memorization, the quality of the samples synthesized by the second model trained on refined synthetic data can be compromised. Other potential approaches to mitigate memorization can be using differential private diffusion models [28, 29] or optimizing model capacity [30].

Patient data memorization in diffusion models can have broad implications in applications of generative AI in medicine. In open-data sharing, patients might not be comfortable making their data publicly available, which is one of the core reasons why generative models are deployed for open-data sharing in the first place. Incidentally sharing patient data copies defeats the whole purpose. Furthermore, patient data copies among synthetic images can also be potentially traced back to the original patient leading to patient re-identification. Packhäuser et al. [12] were able to identify two X-ray images from the same patient acquired at different times even when the patient’s conditions altered. Using such approaches, an attacker can use partially available patient information to recover patient data copies among presumed novel synthetic data and recover sensitive clinical information. Another prominent application of generative models is data expansion diversification [1]. In data expansion and diversification, generative models are trained to synthesize novel data and complement the training data with synthetic data for data-hungry AI models. We observed that a high percentage of synthetic data were patient data copies, especially in the 3D datasets. This also brings the data diversification and expansion application of generative models into question.

4 Methods

4.1 Latent Diffusion Models

Latent diffusion models (LDMs) belong to a family of likelihood-based generative models that are designed to learn data distribution $p(x)$ through a gradual denoising process in a low dimensional latent space (see Fig. 9) [20]. The latent space is learned through an autoencoder. Given an image x , the encoder E_{θ_E} projects x onto its low dimensional latent representation z , followed by a back projection onto the original pixel space as \hat{x} . This latent space project reduces computational complexity and enables application on high-resolution images [20]. The autoencoder is trained using a reconstruction loss (\mathcal{L}_{rec}) that enforces the model to learn a meaningful compressed representation, and adversarial (\mathcal{L}_{adv}) and perceptual (\mathcal{L}_{prec}) losses for enhanced perceptual quality of the reconstructed image. The cumulative loss (\mathcal{L}_{com}) can be expressed as a weighted summation of the reconstruction loss with weighting λ_{rec} , adversarial loss with

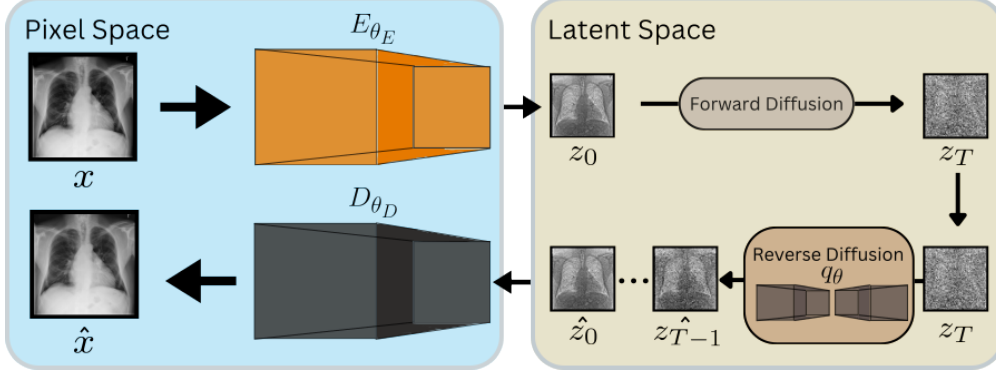


Figure 9: Latent Diffusion Models project data onto a lower dimensional latent space and perform gradual denoising followed by projection back onto the pixel space.

weighting λ_{adv} , and perceptual loss with weighting λ_{perc}

After learning the latent space, deep diffusion models undergo training in the latent space. Deep diffusion models are trained with the aim to minimize the upper variational bound of the negative log-likelihood of the data distribution $-\log(p(z))$ [31]. Training a diffusion model consists of two steps. The first step constitutes a forward diffusion process where normally distributed noise is added to the latent representation z of images x . This process is performed in small increments (δt) with a variance schedule of (β_t) , resulting in noisy representations z_t at every value of t . At any time t , $q(z_t|z_{t-1})$ is modelled as a normal distribution with mean $\sqrt{1-\beta_t}z_{t-1}$ and variance β_t . The second step consists of a reverse diffusion process aimed at learning $q(z_{t-1}|z_t)$. Unlike $q(z_t|z_{t-1})$, $q(z_{t-1}|z_t)$ does not have a closed form expression and is typically estimated using a deep neural network $\hat{q}_{\theta}(z_{t-1}|z_t)$ at various different values of t .

Once the models are trained, they can be used to generate samples by initiating from random noise $z_T \sim \mathcal{N}(0, I)$ and performing sequential denoising to obtain a new sample \hat{z}'_0 in the latent space. This new latent sample can be projected back to the pixel space using the decoder D_{θ_D} .

4.2 Memorization Assessment

Despite the ability of latent diffusion models to generate high-quality and realistic samples, the affinity of such models to memorize patient data and synthesize it has received little attention [13, 18, 26]. Akbar et al. [26] defined memorization as a phenomenon where generative models synthesize patient data copies and defined copies as synthesized samples that are identical to training samples. Dar et al. [18] further expanded the definition of copies to further include variations such as rotation, flipping, and minor changes in contrast. Here we adhere to this expanded definition, and drawing inspiration from Fernandez et al. [27] we formally define memorization as follows:

A training data sample x is considered to be (l, ρ) -memorized by a generative model G_{θ} if $l(x, v(\hat{x})) \geq \tau$, where \hat{x} is a sample extracted from G_{θ} using sampling algorithm A , v corresponds to minor variations such rotation, flipping and slight changes in contrast, l is the similarity between the samples, and τ is a threshold level. Under such conditions, \hat{x} is defined as a copy of x .

4.2.1 Contrastive Learning

One naive way to detect patient data copies is to compare each synthesized sample with all training samples and select the samples showing a similarity level greater than the threshold τ as copies. However, this approach is computationally inefficient and is not suitable for detecting copies that are variations of patient images. Accordingly, we utilized self-supervised models (SS_{θ}) that project images into a lower dimensional embedding space and used a contrastive learning approach [32] to bring each training sample closer to its variation and push away from other samples (Fig. 10). The rationale behind this approach is that copies would lie closer to the training samples and novel samples would be far away. The details of the model are mentioned in Section S1.1

4.2.2 Copy Detection

For the detection of patient data copies, SS_{θ} was first utilized to obtain embeddings of all training, validation, and synthetic samples. Next, Pearson’s correlation coefficient was computed between all pairs of training-validation

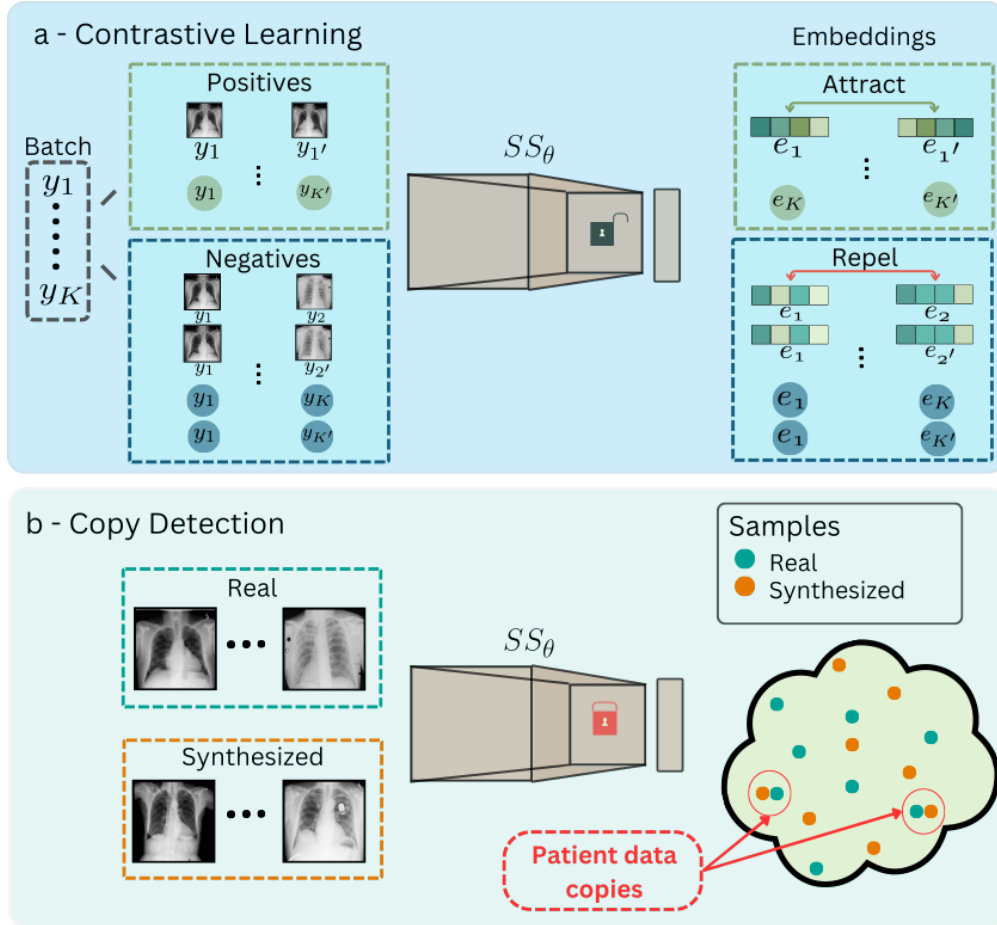


Figure 10: a - Self-supervised model is trained to project images onto a lower dimensional embedding space where each sample within a batch is brought closer to its variation and pushed far away from all other samples in the batch. b - Patient data copies are detected by projecting all training and synthetic samples onto the embedding space and identifying the training synthetic pairs lying close to each other.

embeddings (ρ_{tr-val}), and training-synthetic embeddings (ρ_{tr-syn}). Afterwards, for each training embedding, the closest validation embedding was selected to form a distribution of their correlation values (ρ_{NN-val}). A threshold value (τ) was then defined as 95th percentile of ρ_{NN-val} . Finally, for each training embedding the closest synthetic embedding was selected (ρ_{NN-syn}), and training samples with ρ_{NN-syn} greater than τ were categorized as memorized. Algorithm S1 demonstrates the copy detection process via a pseudo code.

4.3 Training and Evaluation Procedures

For the 3D datasets, two models were considered (MedDiff [24] and MONAI[25]). We opted for these models because they are some of the most widely used repositories for medical image synthesis using latent diffusion models. Training procedures, network architectures, and hyperparameters for MedDiff were adopted from Khader et al. [24] (<https://github.com/FirasGit/medicaldiffusion>) and for MONAI were adopted from the online repository of Pinaya et al. [25] (https://github.com/Project-MONAI/tutorials/blob/main/generative/3d_ldm/config/config_train_32g.json). The only exception was the batch size of the models, which was modified to 8 for the autoencoder and 20 for the diffusion model. MedDiff consisted of a vector quantized generative adversarial network (VQ-GAN) with 3D convolutions as the autoencoder and MONAI consisted of a variational autoencoder (VAE) with 3D convolutions as the autoencoder. All 3D-LDMs were trained for 150k iterations, and the number of sampling time steps was set to 300 in MedDiff and 1000 in MONAI. For the 2D X-ray dataset, training procedures, network architectures, and hyperparameters were adopted from an online repository (https://github.com/Warvito/generative_chestxray) built on the MONAI framework [25], and is referred to as MONAI-2D. MONAI-2D consisted of VAE with 2D convolutions as the autoencoder. All 2D-LDMs were trained for

200k iterations unless specified, and the number of sampling time steps was set to 1000.

In 3D-self supervised models, the architecture of the encoder was modified from the encoder of VQ-VAE in MedDiff. The network was used to reduce the input dimensions to 4^3 and 8 channels, followed by flattening and using dense layers to reduce the dimensions to a 32×1 vector. The training procedures were adopted from Dar et al. [18] In 2D self-supervised models, the model was adopted from Packhäuser et al. [12] with minor modifications in architecture. The last classification layer was replaced by a dense layer having dimensions of 128×1 as output. The training procedures were adopted from Dar et al. [13].

In all synthesized datasets FID and MS-SSIM were adopted from the MONAI repository (<https://github.com/Project-MONAI/GenerativeModels/tree/main/generative/metrics>). In 3D datasets, FID was calculated between features extracted from whole datasets. The features for FID calculation were extracted using a pre-trained model adapted from Chen et al [33]. In the 2D dataset, FID was calculated in batches with a batch size of 256 and averaged afterwards. The features for FID calculation were extracted using a pre-trained model adopted from Cohen et al. [34]. The reported average MS-SSIM values were calculated by computing MS-SSIM values between each synthetic sample and a randomly selected synthetic sample and averaging them.

PCCTA data were acquired at the University Hospital Mannheim on a Siemens Naeotom Alpha scanner. Ethics approval was granted by the Ethics Committee of Ethikkommission II at Heidelberg University (ID 2021-659). In the PCCTA dataset, sub-volumes of sizes 64^3 surrounding coronary artery plaques were cropped. In the MRNet dataset, all volumes were cropped or zero-padded to have sizes of $256^2 \times 32$. In the X-ray dataset, all images were sampled to sizes of 512^2 .

Data Availability: This study utilizes three datasets. The MRNet and X-ray datasets are publicly available at <https://stanfordmlgroup.github.io/competitions/mrnet/> and <https://www.kaggle.com/datasets/nih-chest-xrays/data> respectively. The in-house dataset, however, cannot be made publicly available due to restrictions imposed by the University Hospital Mannheim, where the data were acquired.

Code Availability: In adherence to the FAIR principles (findability, accessibility, interoperability, and reusability) in scientific research, all code utilized in this work is publicly available.

The LDMs were trained using code from public repositories. Specifically, MedDiff was trained using code from <https://github.com/FirasGit/medicaldiffusion>. MONAI was trained using code from <https://github.com/Project-MONAI/>, and MONAI-2D utilized code from https://github.com/Warvito/generative_chestxray. Our code for data pre-processing and training and evaluation of self-supervised models for copy detection is made publicly available at <https://github.com/Cardio-AI/memorization-ldm>.

Acknowledgement: S.U.H.D. is supported through state funds approved by the State Parliament of Baden-Württemberg for the Innovation Campus Health + Life Science Alliance Heidelberg Mannheim.

S.F. is supported by the German Federal Ministry of Education and Research (SWAG, 01KD2215C), the German Cancer Aid (DECADE, 70115166) and the German Research Foundation (504101714).

J.N.K. is supported by the German Cancer Aid (DECADE, 70115166), the German Federal Ministry of Education and Research (PEARL, 01KD2104C; CAMINO, 01EO2101; SWAG, 01KD2215A; TRANSFORM LIVER, 031L0312A; TANGERINE, 01KT2302 through ERA-NET Transcan), the German Academic Exchange Service (SECAI, 57616814), the German Federal Joint Committee (TransplantKI, 01VSF21048) the European Union’s Horizon Europe and innovation programme (ODELIA, 101057091; GENIAL, 101096312), the European Research Council (ERC; NADIR, 101114631) and the National Institute for Health and Care Research (NIHR, NIHR203331) Leeds Biomedical Research Centre. The views expressed are those of the author(s) and not necessarily those of the NHS, the NIHR or the Department of Health and Social Care. This work was funded by the European Union. Views and opinions expressed are however those of the author(s) only and do not necessarily reflect those of the European Union. Neither the European Union nor the granting authority can be held responsible for them.

S.E. is supported by BMBF-SWAG Project 01KD2215D, Carl-Zeiss-Stiftung within the Multi-dimensionAI consortium, and Informatics for Life project through the Klaus Tschira Foundation.

The authors also gratefully acknowledge the data storage service SDS@hd supported by the Ministry of Science, Research and the Arts Baden-Württemberg (MWK) and the German Research Foundation (DFG) through grant INST 35/1314-1 FUGG and INST 35/1503-1 FUGG. The authors also acknowledge support by the state of Baden-Württemberg through bwHPC and the German Research Foundation (DFG) through grant INST 35/1597-1 FUGG.

Conflict of interest: S.O.S. is the director of the Dept. of Radiology and Nuclear Medicine at the University Medical Center in Mannheim, which has research agreements with Siemens Healthineers.

B.B. is the founder and CEO of LernRad GmbH and a speaker at Bureau Bayer Vital GmbH.

S.F. has received honoraria by MSD and BMS.

D.T. holds shares in StratifAI GmbH and has received honoraria for lectures from Bayer.

J.N.K. declares consulting services for Owkin, France; DoMore Diagnostics, Norway; Panakeia, UK; AstraZeneca,

UK; Scailyte, Switzerland; Mindpeak, Germany; and MultiplexDx, Slovakia. Furthermore he holds shares in StratifAI GmbH, Germany, has received a research grant by GSK, and has received honoraria by AstraZeneca, Bayer, Eisai, Janssen, MSD, BMS, Roche, Pfizer and Fresenius. S.E. has received honoraria by Boehringer Ingelheim.

Author Contribution: S.U.H.D. and S.E. developed the ideas for the study and initiated the project. J.K., I.A., and S.O.S. acquired the photon-counting computed tomography angiography dataset, performed pre-processing, and labeled the regions containing plaques. S.U.H.D., M.S., and S.E. designed methodology and experiments. S.U.H.D. and M.S. performed all experiments, and wrote the codes for all experiments. S.U.H.D., M.S., J.N.K., and S.E. interpreted the results. S.U.H.D. and S.E. wrote the manuscript. T.P., S.O.S, N.F., B.B., S.F., D.T., J.N.K., and S.E. guided the study and provided feedback throughout the manuscript preparation.

References

- [1] I. Ktena, O. Wiles, I. Albuquerque, S.-A. Rebuffi, R. Tanno, A. G. Roy, S. Azizi, D. Belgrave, P. Kohli, T. Cemgil *et al.*, “Generative models improve fairness of medical classifiers under distribution shifts,” *Nature Medicine*, pp. 1–8, 2024.
- [2] A. Güngör, S. U. Dar, Şaban Öztürk, Y. Korkmaz, H. A. Bedel, G. Elmas, M. Ozbey, and T. Çukur, “Adaptive diffusion priors for accelerated mri reconstruction,” *Medical Image Analysis*, p. 102872, 2023.
- [3] J. Wolleb, F. Bieder, R. Sandkühler, and P. C. Cattin, “Diffusion models for medical anomaly detection,” in *Medical Image Computing and Computer Assisted Intervention – MICCAI 2022*, L. Wang, Q. Dou, P. T. Fletcher, S. Speidel, and S. Li, Eds. Cham: Springer Nature Switzerland, 2022, pp. 35–45.
- [4] A. Kazerouni, E. K. Aghdam, M. Heidari, R. Azad, M. Fayyaz, I. Hacıhaliloglu, and D. Merhof, “Diffusion models in medical imaging: A comprehensive survey,” *Medical Image Analysis*, vol. 88, p. 102846, 2023.
- [5] W. H. L. Pinaya, P.-D. Tudosiu, J. Dafflon, P. F. Da Costa, V. Fernandez, P. Nachev, S. Ourselin, and M. J. Cardoso, “Brain Imaging Generation with Latent Diffusion Models,” in *Deep Generative Models*. Cham: Springer Nature Switzerland, 2022, pp. 117–126.
- [6] M. Guillaudoux, O. Rousseau, J. Petot, Z. Bennis, C.-A. Dein, T. Goronflot, N. Vince, S. Limou, M. Karakachoff, M. Wargny *et al.*, “Patient-centric synthetic data generation, no reason to risk re-identification in biomedical data analysis,” *NPJ Digital Medicine*, vol. 6, no. 1, p. 37, 2023.
- [7] J.-N. Eckardt, W. Hahn, C. Röllig, S. Stasik, U. Platzbecker, C. Müller-Tidow, H. Serve, C. D. Baldus, C. Schlie-mann, K. Schäfer-Eckart *et al.*, “Mimicking clinical trials with synthetic acute myeloid leukemia patients using generative artificial intelligence,” *NPJ digital medicine*, vol. 7, no. 1, p. 76, 2024.
- [8] A. Zhang, L. Xing, J. Zou, and J. C. Wu, “Shifting machine learning for healthcare from development to deployment and from models to data,” *Nature Biomedical Engineering*, vol. 6, no. 12, pp. 1330–1345, 2022.
- [9] A. DuMont Schütte, J. Hetzel, S. Gatidis, T. Hepp, B. Dietz, S. Bauer, and P. Schwab, “Overcoming barriers to data sharing with medical image generation: a comprehensive evaluation,” *NPJ digital medicine*, vol. 4, no. 1, p. 141, 2021.
- [10] I. E. Hamamci, S. Er, E. Simsar, A. Tezcan, A. G. Simsek, F. Almas, S. N. Esirgun, H. Reynaud, S. Pati, C. Bluethgen *et al.*, “Generatect: Text-guided 3d chest ct generation,” *arXiv preprint arXiv:2305.16037*, 2023.
- [11] P. Chambon, C. Bluethgen, J.-B. Delbrouck, R. Van der Sluijs, M. Połacin, J. M. Z. Chaves, T. M. Abraham, S. Purohit, C. P. Langlotz, and A. Chaudhari, “Roentgen: Vision-language foundation model for chest x-ray generation,” 2022. [Online]. Available: <https://arxiv.org/abs/2211.12737>
- [12] K. Packhäuser, S. Gundel, N. Münster, C. Syben, V. Christlein, and A. Maier, “Deep learning-based patient re-identification is able to exploit the biometric nature of medical chest x-ray data,” *Scientific Reports*, vol. 12, no. 1, p. 14851, 2022.
- [13] S. U. H. Dar, I. Ayx, M. Kapusta, T. Papavassiliou, S. O. Schoenberg, and S. Engelhardt, “Effect of training epoch number on patient data memorization in unconditional latent diffusion models,” in *Bildverarbeitung für die Medizin 2024*, 2024.
- [14] M. Heusel, H. Ramsauer, T. Unterthiner, B. Nessler, and S. Hochreiter, “Gans trained by a two time-scale update rule converge to a local nash equilibrium,” in *Advances in Neural Information Processing Systems*,

- I. Guyon, U. V. Luxburg, S. Bengio, H. Wallach, R. Fergus, S. Vishwanathan, and R. Garnett, Eds., vol. 30. Curran Associates, Inc., 2017. [Online]. Available: https://proceedings.neurips.cc/paper_files/paper/2017/file/8a1d694707eb0fefe65871369074926d-Paper.pdf
- [15] Z. Wang, E. Simoncelli, and A. Bovik, “Multiscale structural similarity for image quality assessment,” in *The Thirty-Seventh Asilomar Conference on Signals, Systems & Computers, 2003*, vol. 2, 2003, pp. 1398–1402 Vol.2.
- [16] A. Borji, “Pros and cons of gan evaluation measures: New developments,” *Computer Vision and Image Understanding*, vol. 215, p. 103329, 2022. [Online]. Available: <https://www.sciencedirect.com/science/article/pii/S1077314221001685>
- [17] N. Carlini, C. Liu, Ú. Erlingsson, J. Kos, and D. Song, “The secret sharer: Evaluating and testing unintended memorization in neural networks,” in *28th USENIX Security Symposium (USENIX Security 19)*. Santa Clara, CA: USENIX Association, Aug. 2019, pp. 267–284. [Online]. Available: <https://www.usenix.org/conference/usenixsecurity19/presentation/carlini>
- [18] S. U. H. Dar, A. Ghanaat, J. Kahmann, I. Ayx, T. Papavassiliu, S. O. Schoenberg, and S. Engelhardt, “Investigating data memorization in 3d latent diffusion models for medical image synthesis,” in *Deep Generative Models*, A. Mukhopadhyay, I. Oksuz, S. Engelhardt, D. Zhu, and Y. Yuan, Eds. Cham: Springer Nature Switzerland, 2024, pp. 56–65.
- [19] G. Somepalli, V. Singla, M. Goldblum, J. Geiping, and T. Goldstein, “Diffusion art or digital forgery? investigating data replication in diffusion models,” in *Proceedings of the IEEE/CVF Conference on Computer Vision and Pattern Recognition (CVPR)*, June 2023, pp. 6048–6058.
- [20] R. Rombach, A. Blattmann, D. Lorenz, P. Esser, and B. Ommer, “High-Resolution Image Synthesis with Latent Diffusion Models,” in *2022 IEEE/CVF Conference on Computer Vision and Pattern Recognition (CVPR)*, 2022, pp. 10 674–10 685.
- [21] L. Zhang, A. Rao, and M. Agrawala, “Adding conditional control to text-to-image diffusion models,” in *2023 IEEE/CVF International Conference on Computer Vision (ICCV)*, 2023, pp. 3813–3824.
- [22] N. Bien, P. Rajpurkar, R. L. Ball, J. Irvin, A. Park, E. Jones, M. Bereket, B. N. Patel, K. W. Yeom, K. Shpanskaya, S. Halabi, E. Zucker, G. Fanton, D. F. Amanatullah, C. F. Beaulieu, G. M. Riley, R. J. Stewart, F. G. Blankenberg, D. B. Larson, R. H. Jones, C. P. Langlotz, A. Y. Ng, and M. P. Lungren, “Deep-learning-assisted diagnosis for knee magnetic resonance imaging: Development and retrospective validation of mrnet,” *PLOS Medicine*, vol. 15, no. 11, pp. 1–19, 11 2018.
- [23] X. Wang, Y. Peng, L. Lu, Z. Lu, M. Bagheri, and R. M. Summers, “Chestx-ray8: Hospital-scale chest x-ray database and benchmarks on weakly-supervised classification and localization of common thorax diseases,” in *Proceedings of the IEEE Conference on Computer Vision and Pattern Recognition (CVPR)*, July 2017.
- [24] F. Khader, G. Müller-Franzes, S. Tayebi Arasteh, T. Han, C. Haarbuerger, M. Schulze-Hagen, P. Schad, S. Engelhardt, B. Baeßler, S. Foersch, J. Stegmaier, C. Kuhl, S. Nebelung, J. N. Kather, and D. Truhn, “Denosing diffusion probabilistic models for 3D medical image generation,” *Scientific Reports*, vol. 13, no. 1, p. 7303, 2023.
- [25] W. H. Pinaya, M. S. Graham, E. Kerfoot, P.-D. Tudosiu, J. Dafflon, V. Fernandez, P. Sanchez, J. Wolleb, P. F. da Costa, A. Patel *et al.*, “Generative ai for medical imaging: extending the monai framework,” *arXiv preprint arXiv:2307.15208*, 2023.
- [26] M. U. Akbar, W. Wang, and A. Eklund, “Beware of diffusion models for synthesizing medical images—a comparison with gans in terms of memorizing brain tumor images,” *arXiv preprint arXiv:2305.07644*, 2023.
- [27] V. Fernandez, P. Sanchez, W. H. L. Pinaya, G. Jacenków, S. A. Tsiftaris, and J. Cardoso, “Privacy distillation: Reducing re-identification risk of multimodal diffusion models,” *arXiv preprint arXiv:2306.01322*, 2023.
- [28] T. Dockhorn, T. Cao, A. Vahdat, and K. Kreis, “Differentially Private Diffusion Models,” *Transactions on Machine Learning Research*, 2023. [Online]. Available: <https://openreview.net/forum?id=ZPpQk7FJXF>
- [29] M. Tölle, U. Köthe, F. André, B. Meder, and S. Engelhardt, “Content-aware differential privacy with conditional invertible neural networks,” in *Distributed, Collaborative, and Federated Learning, and Affordable AI and Healthcare for Resource Diverse Global Health*. Cham: Springer Nature Switzerland, 2022, pp. 89–99.
- [30] R. Dutt, P. Sanchez, O. Bohdal, S. A. Tsiftaris, and T. Hospedales, “Memcontrol: Mitigating memorization in medical diffusion models via automated parameter selection,” 2024.
- [31] J. Ho, A. Jain, and P. Abbeel, “Denosing Diffusion Probabilistic Models,” in *Advances in Neural Information Processing Systems*, H. Larochelle, M. Ranzato, R. Hadsell, M. F. Balcan, and H. Lin, Eds., vol. 33. Curran Associates, Inc., 2020, pp. 6840–6851.

- [32] T. Chen, S. Kornblith, M. Norouzi, and G. Hinton, “A simple framework for contrastive learning of visual representations,” in *Proceedings of the 37th International Conference on Machine Learning*, ser. Proceedings of Machine Learning Research, H. D. III and A. Singh, Eds., vol. 119. PMLR, 13–18 Jul 2020, pp. 1597–1607. [Online]. Available: <https://proceedings.mlr.press/v119/chen20j.html>
- [33] S. Chen, K. Ma, and Y. Zheng, “Med3d: Transfer learning for 3d medical image analysis,” *arXiv preprint arXiv:1904.00625*, 2019.
- [34] J. P. Cohen, J. D. Viviano, P. Bertin, P. Morrison, P. Torabian, M. Guarrera, M. P. Lungren, A. Chaudhari, R. Brooks, M. Hashir, and H. Bertrand, “Torchxrayvision: A library of chest x-ray datasets and models,” in *Proceedings of The 5th International Conference on Medical Imaging with Deep Learning*, ser. Proceedings of Machine Learning Research, E. Konukoglu, B. Menze, A. Venkataraman, C. Baumgartner, Q. Dou, and S. Albarqouni, Eds., vol. 172. PMLR, 06–08 Jul 2022, pp. 231–249. [Online]. Available: <https://proceedings.mlr.press/v172/cohen22a.html>

Supplementary Material

S1 Supplementary Methods

S1.1 Self-Supervised Model Training

Consider a batch $B = [y_1, y_2, \dots, y_K]$ containing K samples, where y_i corresponds to i^{th} sample. After obtaining variation y'_i for each sample y_i , the modified batch can then be represented as $B' = [y_1, y'_1, y_2, y'_2, \dots, y_K, y'_K]$. One straightforward way is to form a positive (y_i, y'_i) and a negative pair (y_i, y_j) for each sample y_i . However, we observed that such an approach was unable to efficiently push samples within a negative pair away from each other. Therefore we increased the number of negative pairs for each sample, such that for each sample y_i negative pairs were formed using all other samples in the batch, making $2(K - 1)$ negative pairs per sample.

The self-supervised model SS_θ model was trained using the normalized temperature-scaled cross entropy (NT-Xent) loss [32]. First, SS_θ was used to obtain embeddings $E = [e_1, e'_1, e_2, e'_2, \dots, e_K, e'_K]$ of all samples within B' . For each i^{th} sample it was then updated based on the NT-Xent loss function, expressed as follows:

$$\mathcal{L}_i = -\log \frac{e^{(s_{e_i, e'_i} / \tau)}}{\sum_{j=1}^{2K} \mathbb{1}_{[j \neq i]} e^{(s_{e_i, e_j} / \tau)}} + \frac{e^{(s_{e'_j, e_j} / \tau)}}{\sum_{j=1}^{2K} \mathbb{1}_{[j \neq i']} e^{(s_{e_{i'}, e_j} / \tau)}} \quad (1)$$

Here $s_{e_{i'}, e_j}$ is cosine similarity i^{th} and j^{th} embeddings and $\mathbb{1}_{[j \neq i]}$ is the indicator function which is 1 when $j \neq i$ and 0 when $j = i$.

Algorithm S1: Copy detection

Input: $E_{tr} = [e_{tr}^1, \dots, e_{tr}^{N_{tr}}]^T \in \mathbb{R}^{N_{tr} \times L}$: N_{tr} training embeddings of length L

$E_{val} = [e_{val}^1, \dots, e_{val}^{N_{val}}]^T \in \mathbb{R}^{N_{val} \times L}$: N_{val} validation embeddings

$E_{syn} = [e_{syn}^1, \dots, e_{syn}^{N_{syn}}]^T \in \mathbb{R}^{N_{syn} \times L}$: N_{syn} synthetic embeddings

$corr(., .)$: Pearson's correlation between inputs

$percentile(., u)$: u th percentile of input vector

$ind()$: Indices of True values

Output: ID_{cop} : Indices of memorized samples

- 1 $\rho_{tr-val} = corr(E_{tr}, E_{val}) \in \mathbb{R}^{N_{tr} \times N_{val}}$ // Pairwise correlations between embeddings
 - 2 $\rho_{tr-syn} = corr(E_{tr}, E_{syn}) \in \mathbb{R}^{N_{tr} \times N_{syn}}$
 - 3 $\rho_{NN-val} = max(\rho_{tr-val}) \in \mathbb{R}^{N_{tr}}$ // Nearest neighbor selection for each training embedding
 - 4 $\rho_{NN-syn} = max(\rho_{syn-val}) \in \mathbb{R}^{N_{tr}}$
 - 5 $\tau = percentile(\rho_{NN-val}, 95)$ // Threshold based on 95 percentile
 - 6 $ID_{cop} = ind(\rho_{NN-syn} \geq \tau)$ // Indices of training samples that are memorized
-

S2 Supplementary Figures

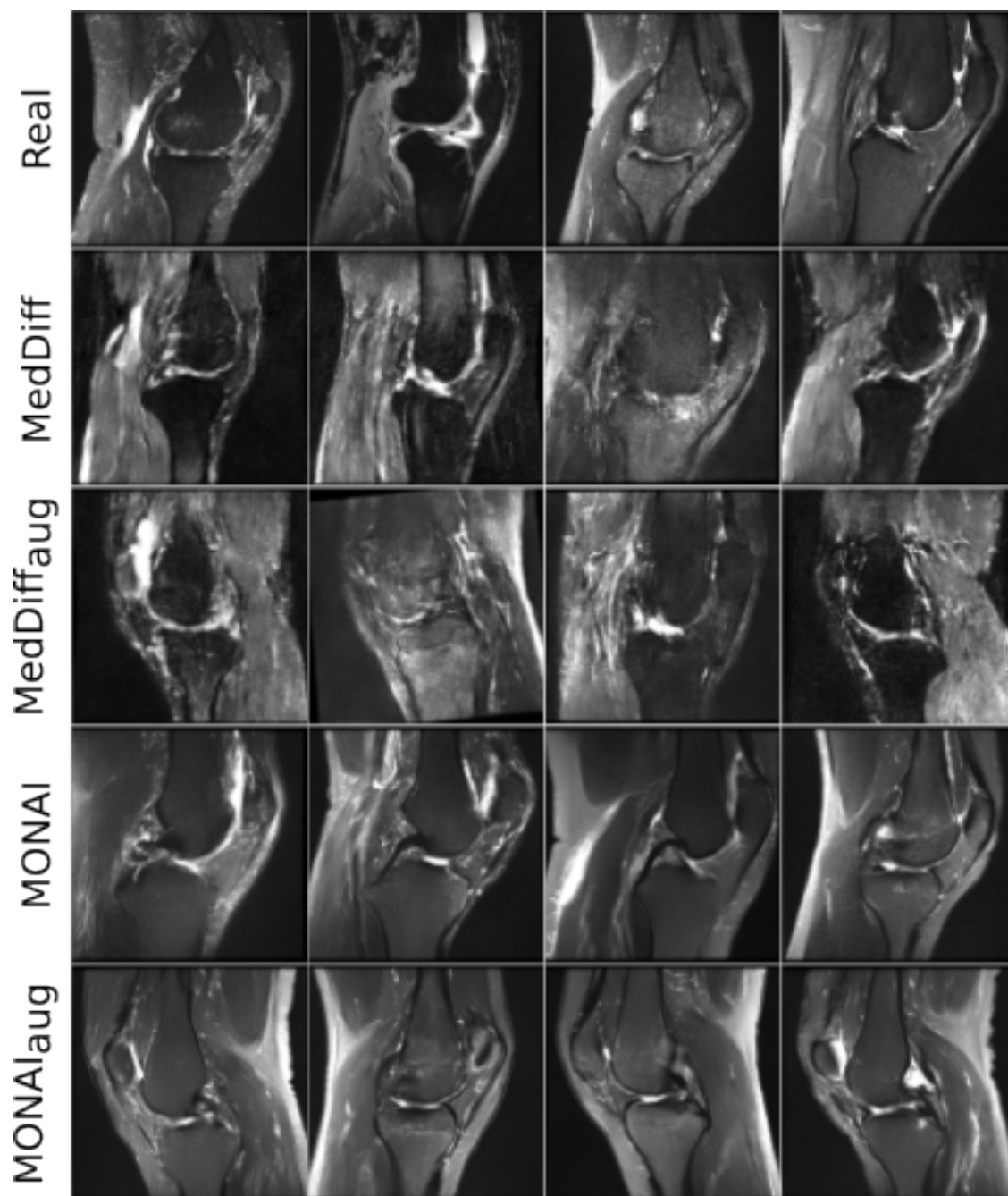


Figure S1: Central slices of randomly selected real samples are shown along with central slices of randomly selected MedDiff-synthesized, MedDiff_{aug}-synthesized, MONAI-synthesized, and MONAI_{aug}-synthesized samples. MedDiff-synthesized samples are noisy and are unable to produce finer structural details. MedDiff_{aug}-synthesized samples are noisier and not realistic. MONAI-synthesized and MONAI_{aug}-synthesized samples are more realistic but are blurry.

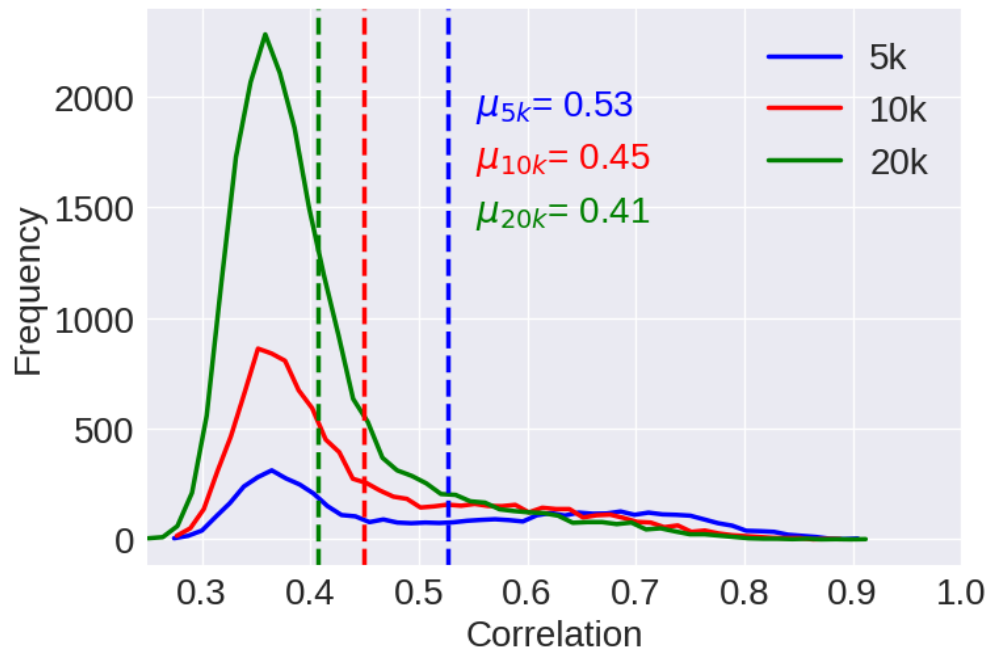


Figure S2: Effect of training data size on memorization. Separate models were trained on 5k ($G_{\theta,5k}$), 10 ($G_{\theta,10k}$), and 20k ($G_{\theta,20k}$) images. Distributions of Pearson's correlation coefficient between training and nearest synthetic samples for $G_{\theta,5k}$, $G_{\theta,10k}$ and $G_{\theta,20k}$ with their respective mean values (μ_{5k} , μ_{10k} and μ_{20k}) are shown. In all cases, the total number of memorized training samples N_{mem} seems similar.

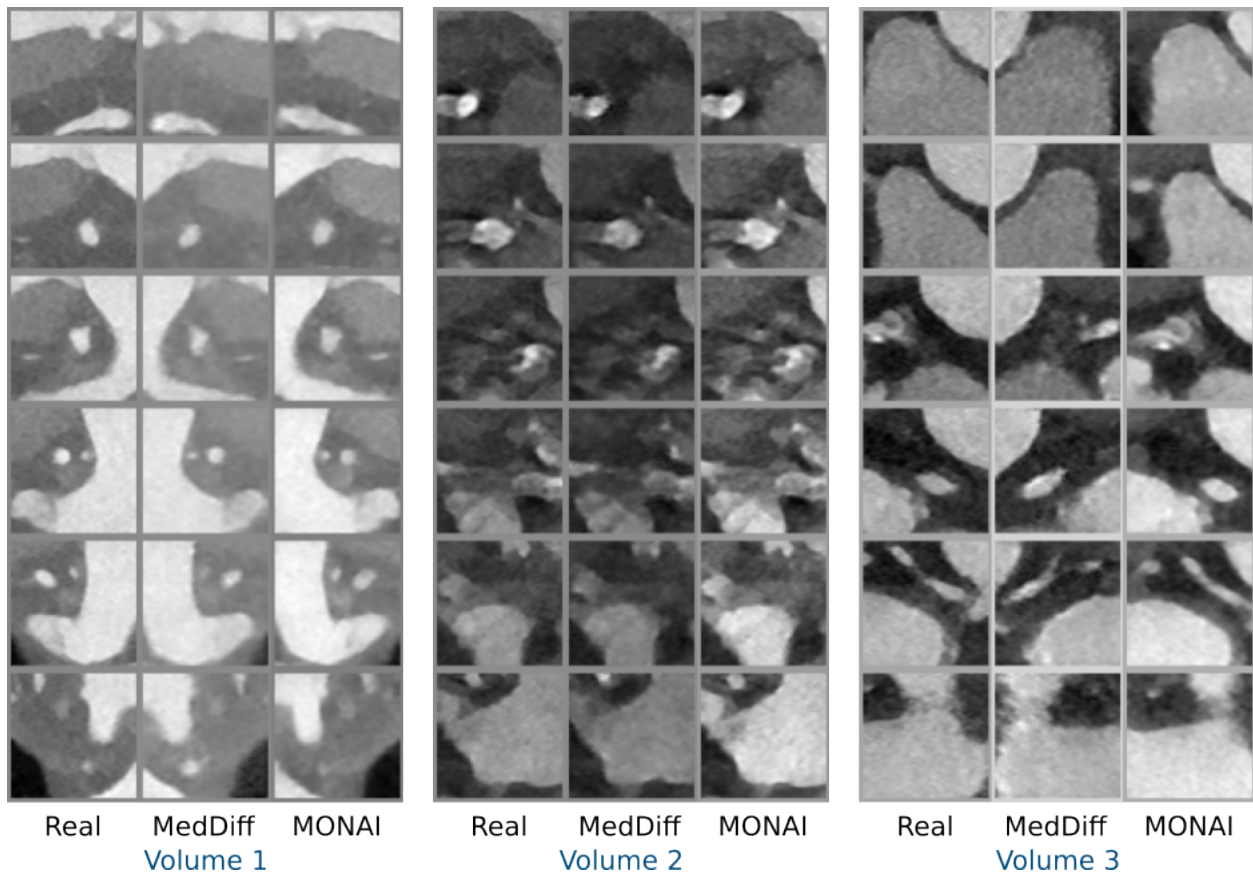


Figure S3: Representative cross sections of real (Real) and copies (MedDiff, MONAI) detected in the PCCTA dataset.

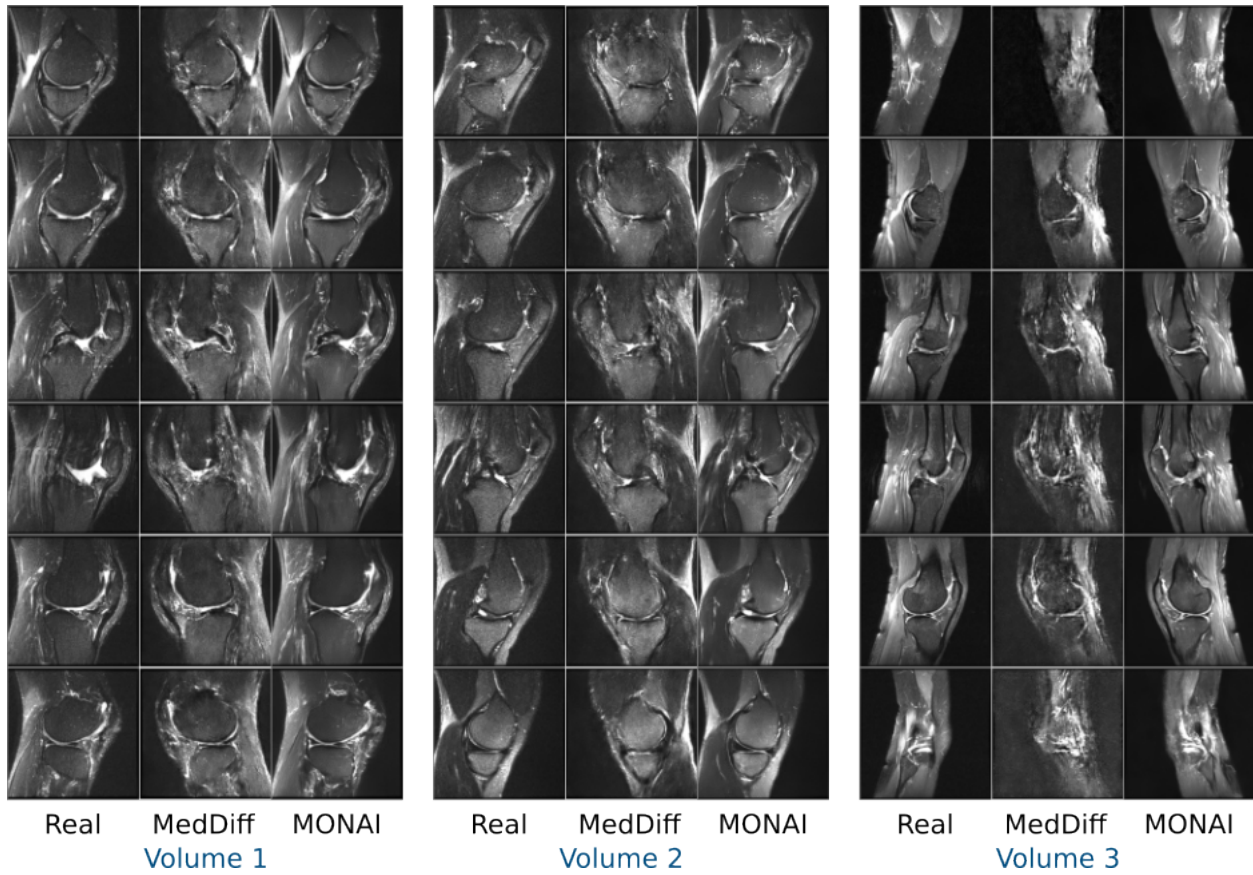


Figure S4: Representative cross sections of real (Real) and copies (MedDiff, MONAI) detected in the MRNet dataset.

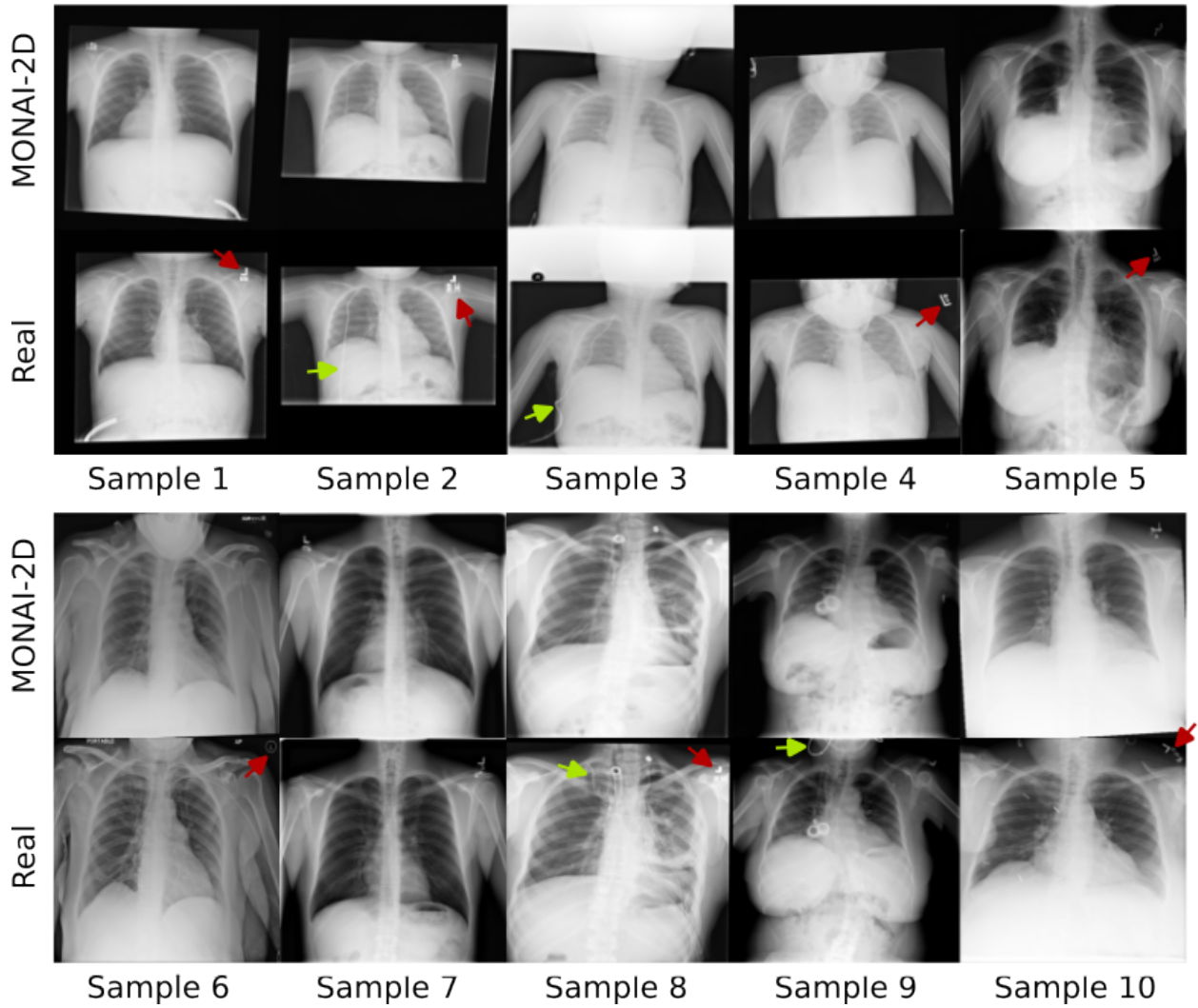


Figure S5: Representative cross sections of real (Real) and copies (MONAI-2D) detected in the X-ray dataset. The augmented model generates copies that in addition to augmentations also produce minor variations (marked with arrows).